Available online at www.sciencedirect.com
SCIENCE DIRECT®
International Journal of Multiphase Flow 32 (2006) 661–676
International Journal of Multiphase Flow
www.elsevier.com/locate/ijmulflow

Spontaneous radial capillary impregnation across a bank of aligned micro-cylinders – Part I: Theory and model development

V. Neacsu [a,b], A. Abu Obaid [b], S.G. Advani [a,b,*]

[a] Department of Mechanical Engineering, University of Delaware, 126 SPL, Newark DE 19716, USA
[b] Center for Composite Materials, University of Delaware, 201 CCM, Newark DE 19716, USA

Received 29 August 2005; received in revised form 7 February 2006

Abstract

This paper presents an analytical and numerical approach to describe the capillary infusion of a liquid across an array of parallel micro-cylinders. Based on a series of simplifying assumptions, the model proposes a method to average the varying capillary pressure and introduces a technique to assess the inhibiting effects of the gas entrapped between the micro-cylinders as the liquid radially ingresses into the micro-cylinder array. The proposed averaging scheme of the capillary pressure is an improvement over previous analytical approaches, as it accounts for the physics of wetting at the micro-scale. The equations are non-dimensionalized and the role of various parameters such as gas entrapment and average capillary pressure is explored. The inclusion of the gas displacement phenomenon requires only one parameter to be determined empirically, in order to describe the impregnation behavior of the liquid. Two limiting cases when all gas is allowed to escape through the impregnating liquid and when all the gas is entrapped within are identified. This study should prove useful in understanding the role of entrained gas and capillarity on impregnation mechanics in micro-scale porous media.

Keywords: Multiphase flows; Flows through porous media; Capillary flows; Micro-scale phenomena

1. Introduction

The role of capillarity in permeating micro- and nano-scale pores with a liquid is of general interest. Flow of liquids around micro- and nano-structures or through small-scale pores is a common occurrence in increasingly numerous engineering applications such as dyeing, papermaking, composite manufacturing, electronic microcircuits assembly and in membranes employed in medical and pharmaceutical industries. Thus, there is a growing need to accurately model capillary driven flows. The significance and characterization of capillary

* Corresponding author. Address: Department of Mechanical Engineering, University of Delaware, 126 SPL, Newark DE 19716, USA. Tel.: +1 302 831 8975; fax: +1 302 831 3619.
E-mail address: advani@me.udel.edu (S.G. Advani).

0301-9322/$ - see front matter
doi:10.1016/j.ijmultiphaseflow.2006.02.006

forces were proposed early in the 20th century and some of the approaches, (e.g. Lucas, 1918; Washburn, 1921) are commonly used today.

The permeation can be seen as flow of two immiscible phases through a complex domain (Kaviany, 1995). One of the phases is a gas (usually air), which gets displaced by or dissolved in the liquid as the liquid (the second phase) permeates the void spaces. The boundary surface delimiting the volumes occupied by the two phases can be extremely irregular, usually defining a multiple connected 3D domain (Greenberg, 1998). We specifically focus on transverse permeation of liquid across a circular bundle of micro-cylinders. The modeling of the boundary condition at the gas–liquid interface usually will determine the degree of accuracy with which the infusion rate of liquid in the bundle of micro-cylinders is estimated. One aspect not adequately addressed by the existing literature is the influence of the entrapped gas on the impregnation of the liquid across an array of micro-cylinders due to the capillary effect.

Another feature of the physics of permeation with no externally imposed pressure gradient is that the liquid motion is driven primarily by the difference in pressure due to the capillary effect. As the flow is slow and one can assume the bundle of cylinders to form the porous media, this allows one to use Darcy (1856) equation, to describe the transversal infusion process. The properties of the gas–liquid interface will play a crucial role in defining the pressure value on the moving boundary and this paper will explore the importance of this relationship.

In the following sections, we present a model to describe radial capillary infusion of a viscous liquid inside a quasi-homogeneous porous cylindrical structure, which consists of an aligned array of micro-cylinders. The influence of the displacement or dissolution of gas within the porous media is also incorporated. Focus is then placed on particular cases of the general problem. Results predicting the flow behavior at micro-scale level for the simplified case are derived in non-dimensional form (flow front radius versus time, variation of pressure and flow velocity within the liquid domain). Additionally, a numerical application of the general model is presented to give a better understanding of how local variation of micro-cylinder volume fraction may influence the overall impregnation dynamics.

Our approach should prove useful to understand and characterize the influence of various parameters pertaining to the permeable media (porosity, permeability), the permeating liquid (surface tension, viscosity), and the physical environment (external pressure, presence/absence of gas within the permeable media).

2. Background

Capillary driven flows have been of interest in many applications where the flow is modeled as flow through porous media. Researchers have approached the flow at micro-scale level in order to derive interrelations with phenomena at meso- or macro-scale. Multiscale studies on flow through porous media (e.g. Bernet et al., 1999; Binetruy et al., 1997; Dimitrovova and Advani, 2002; Parnas et al., 1994; Pillai and Advani, 1995; Simacek and Advani, 2003) recognize the importance of capillary forces, and account for them in various ways. Capillary effects have been explored with analytical methods (e.g. Bernet et al., 1999; Foley, 2003; Foley and Gillespie, 2005; Pillai and Advani, 1995; Potter, 1997), via numerical techniques (Alazmi and Vafai, 2004; Dimitrovova and Advani, 2002; Pillai and Advani, 1995; Young, 2004), as well as experimentally (Batch et al., 1996; Chwastiak, 1971; Foley and Gillespie, 2005).

This paper presents a model for radial axisymmetric infusion of viscous liquids across a bank of aligned micro-cylinders. Our approach differs from others (e.g. Ahn et al., 1991; Bernet et al., 1999; Foley, 2003) in calculation of the capillary pressure at the micro-scale level, and the averaging method used at the level of the porous structure. Our proposed equation for the average capillary pressure results in lower values as compared to values reported by Ahn et al. (1991), although they are of the same order of magnitude. The problem we are dealing with is slightly similar to that approached by Srinivasan and Vafai (1994), but in that study both fluids displacing each other in a porous medium were incompressible. The present work also introduces a new method to account for the displacement of gas from the porous structure. Although previous studies by Bernet et al. (1999), Foley (2003) and Foley and Gillespie (2005) acknowledged and qualitatively approached the inhibiting effect of gas pressure on the overall behavior of the liquid infusion, a more general methodology is introduced here. Wherever possible throughout the paper, non-dimensional parameters and equations are employed to make it possible to address a wide range of applications.

The specific application that motivated this study is the infusion of fiber bundles (tows) during composite manufacturing processes. In such processes, a fiber preform consists of stitched or woven bundles of fibers (tows) as in textiles. Each bundle is a porous cylinder of millimeter-size elliptical or circular cross-section that holds together thousands of aligned individual fiber strands. The fiber cross-section can be considered circular, and the diameter of the fiber is of the order of a few microns. These fiber preforms are placed in a mold to make the desired part and a viscous resin is infused to fill the empty spaces between the fiber tows and within the fiber tows. The goal is to fill the empty spaces between fibers with the resin, by completely displacing the air present within the fiber bundles, as shown by Gokce et al. (2002), Lawrence (2002) and Liu et al. (1996). One may apply a positive pressure difference to drive the liquid through the gaps between the fibers but it is usually the capillary pressure that infuses the porous cylindrical structure (the fiber tows).

3. Analytical and numerical approach

An analytical model to describe the capillary advancement of flow at micro-scale level allows one to identify important non-dimensional parameters and apply the correct scaling.

3.1. Definitions and basic concepts

We will consider capillary flow across a bank of aligned micro-cylinders, which is a specific case of the two-phase flow model by Kaviany (1995). The two immiscible fluids (gas and liquid) that come in dynamic contact with a solid phase (micro-cylinders) define the solid–liquid, solid–gas, and liquid–gas interfaces. The surface tensions characterizing the three phases determine the geometry of the contact lines formed at the interfaces, specifically the contact surface between the gas and the liquid. Usually, the Young–Dupré condition [Eq. (1)] is used to obtain the value of the contact angle formed by the tangents to the solid–liquid and liquid–gaseous interfaces:

$$\sigma_{gs} - \sigma_{ls} = \sigma_{lg} \cdot \cos\theta_s \tag{1}$$

where σ_{ls}, σ_{gs}, and σ_{lg} denote the surface tensions for the solid–liquid, solid–gas, and liquid–gas interfaces respectively, while θ_s is the static contact angle. However, the process that we are studying is a dynamic one, featuring a different contact angle at the advancing interface. The "advancing contact angle" (θ_a) is always larger than the static contact angle (Kaviany, 1995), and its value is determined experimentally.

3.2. Assumptions and simplifications

Due to the complexity of the problem, the analytical approach is based on several simplifying assumptions. To start with, the porous structure is assumed to be circular, encompassing identical micro-cylinders as shown in Fig. 1. The distribution of the micro-cylinders is assumed quasi-hexagonal, although a variation of the solid volume fraction (ratio of the micro-cylinder volume to the total porous cylinder volume) is allowed to exist in the radial direction, from the outer edge to the center of the porous cylinder. The micro-structure of the porous cylinder will be considered relevant only up to a point (e.g. to obtain the expression of the capillary pressure); nevertheless, for the purpose of deriving flow equations at the scale of the porous macro-cylinder, we will neglect the heterogeneity of the medium, which will be assumed homogeneous and characterized by a hydrodynamic permeability.

In addition, it is assumed that there are no parameters that vary in circumferential or in axial directions; the flow is assumed to advance only in radial direction, transversally to the micro-cylinders orientation, toward the center of the porous structure. During the inward impregnation, it is assumed that the region behind the advancing liquid/gas interface is fully saturated. As a consequence, the flow front (interface) is believed to remain circular at all times, enclosing a completely dry region of the porous material, the region left behind being fully wetted. Temperature is assumed constant in time and uniform throughout the liquid and gaseous domain, density of liquid also remains constant in time. No movement of the micro-cylinders is considered during the impregnation process. Body forces and inertial effects are neglected.

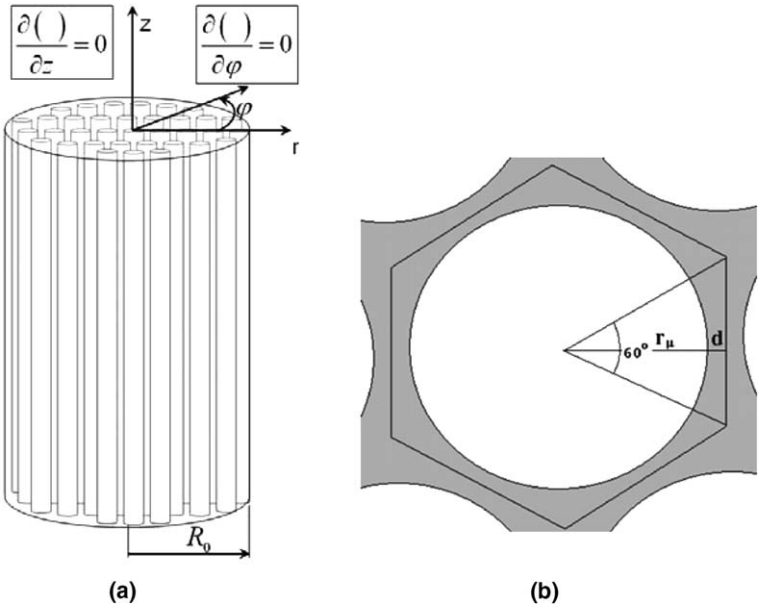

Fig. 1. (a) Cylindrical porous media consisting of solid micro-cylinders arranged in a quasi-hexagonal pattern. The region between the micro-cylinders can be occupied by either gas or liquid. (b) Characteristic geometric parameters defining the arrangement at the micro-scale level (micro-cylinder radius r_μ and half the spacing between two neighboring micro-cylinders, d).

At this point, no other assumptions are made about the variation of other material and process parameters: solid volume fraction and liquid viscosity are allowed to vary in radial direction, while liquid's surface tension, as well as the pressure of the liquid around the porous structure are allowed to vary in time. A consequence of the latter would be that an applied pressure difference might assist the capillary impregnation.

3.3. Permeability of the porous circular domain

There are many models which could be used to estimate the permeability of a porous domain containing micro-cylinders (e.g. Ballata et al., 1999; Calado and Advani, 1996; Nedanov and Advani, 2002; Parnas et al., 1995; Pillai and Advani, 1995; Simacek and Advani, 1996), some particularly applicable to the case of hexagonally arranged micro-cylinders in a circular bundle (Bruschke and Advani, 1993; Dimitrovova and Advani, 2002; Gebart, 1992; Papathanasiou, 2001; Ranganathan et al., 1996; Sadiq et al., 1995). Without choosing a specific model with various approximation, we will only retain the common assumption that the permeability K of the porous medium depends exclusively on the local solid volume fraction V_f:

$$K = K(V_f) \tag{2}$$

3.4. Capillary pressure

Alone or in combination with an applied pressure difference, capillary pressure drives a wetting liquid toward the center of the circular porous domain. Generally, for an irregular interface, the expression of the capillary pressure is

$$p_c = \sigma_{lg} \cdot \left(\frac{1}{r_c^{(1)}} + \frac{1}{r_c^{(2)}} \right) \tag{3}$$

where $r_c^{(1)}$ and $r_c^{(2)}$ are the radii of curvature characterizing the liquid–gas interface.

In the case of capillary flow across aligned micro-cylinders, the assumed geometric configuration renders one of the curvature radii infinite, and therefore the meniscus can be considered as dependent on only one

radius of curvature. Out of the models proposed so far for the capillary pressure, we use the expression proposed by Bayramli and Powell (1990). The proposed equation for capillary pressure, with only minor modifications is as follows:

$$p_c(\alpha) = \frac{\sigma}{r_\mu} \cdot \frac{\cos(\alpha + \theta)}{1 - \cos\alpha + \xi} \tag{4}$$

where σ is the liquid's surface tension, θ is the advancing contact angle, r_μ is the micro-cylinder radius, $\xi = d/r_\mu$ is the relative spacing ratio, and α is a local angular coordinate.

It is important to note that the value of the capillary pressure given by Eq. (4) varies as the meniscus sweeps the range between two limit values of the angular coordinate α (Fig. 2a). The minimum angle α_{inf} is a negative value corresponding to the configuration when the meniscus first touches the surface of the two neighboring micro-cylinders. Correspondingly, the maximum angular coordinate α_{sup} is reached when the flow is transferred to the next concentric layers of micro-cylinders, closer to the center of the porous cylindrical structure.

More suggestive is a qualitative surface plot of the capillary pressure, as a function of the angular coordinate α and the relative spacing ratio ξ, the other parameters being held constant. Eq. (4) was used to generate the plot in Fig. 2b, which shows that capillary pressure is higher at low spacing ratios (i.e. at high values of the solid volume fraction) and near the strait between the two neighboring micro-cylinders.

For a given arrangement of micro-cylinders (known spacing ratio ξ), the analytical integration of the capillary impregnation process can be facilitated by using an overall value of the capillary pressure, instead of the fluctuating capillary pressure, different at every meniscus location. Although we assumed that the macro-flow front advances uniformly toward the center of the porous macro-cylinder, preserving a circular shape, it is realistic to assume that the flow at micro-scale does not develop at the same rate between any two neighboring micro-cylinders located at the same concentric layer (Fig. 3). Therefore, it is reasonable to introduce a mean value of the capillary pressure.

An intuitive way to average the capillary pressure proposed by Foley (2003) is to simply integrate it over the angular interval (α_{inf}; α_{sup}). Due to the fact that the angular interval (α_{inf}; α_{sup}) diminishes for increasing values of the advancing contact angle, the intuitive technique proposed by Foley (2003) produces higher average capillary pressures for less wettable liquids. We propose an alternative approach, which uses a weighting function in the integral of the variable capillary pressure. This correction takes into account the fact that the probability of the meniscus to be located at a particular angular coordinate α is inversely proportional to the instantaneous flow front velocity, therefore directly proportional to the gap between the neighboring micro-cylinders at that location. As the flow front moves slowly near the limits of the integration interval, and faster where the gap is smaller (due to mass conservation considerations), higher values of the capillary pressure at mid-interval should bear a lower significance when computing the average value.

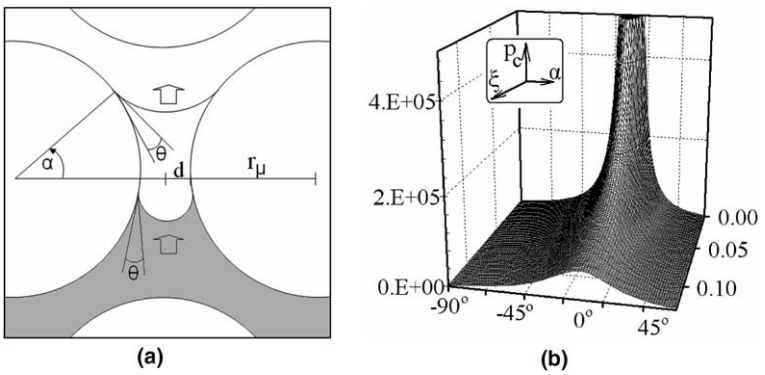

Fig. 2. (a) Progressive motion of the meniscus, between two neighboring micro-cylinders, as the capillary impregnation develops toward the center of the porous structure (upward in the sketch). (b) Capillary pressure as a function of spacing ratio ξ and local angular coordinate α (numerical values are in Pascal units, corresponding to an arbitrarily chosen set of surface tension σ, micro-cylinder radius r_μ, and contact angle θ).

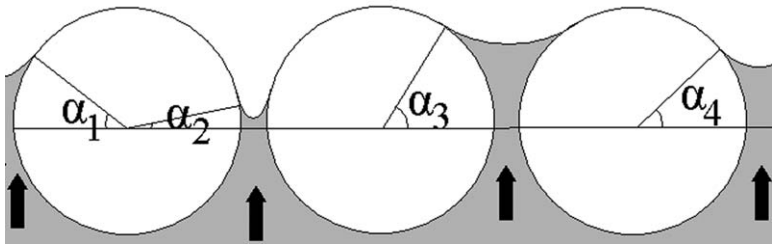

Fig. 3. Random progression of the meniscus, yet on the same concentric layer of micro-cylinders. Neither the local angular coordinates defining the location of the meniscus between neighboring micro-cylinders, nor the curvature radii are the same, which causes local variation of the capillary pressure and the use of mean capillary pressure.

Thus, we calculated the mean capillary pressure by using this weighting function, and is given by

$$\overline{p_c} = \frac{\sigma}{r_\mu} \cdot \frac{\sin(\alpha_{sup} + \theta) - \sin(\alpha_{inf} + \theta)}{\frac{5\pi}{6}(1+\xi) - 1 - \frac{\sqrt{3}}{2}} \tag{5}$$

Finding the specific values of limits α_{sup} and α_{inf} is non-trivial, as they depend on both the advancing contact angle and on the spacing ratio ξ. For this purpose, one needs to consider the jumps of the contact lines from one concentric micro-cylinder layer to the next. Useful comments on this topic, as well as other geometric limitations of transverse capillary impregnation are included in Bayramli and Powell (1990) and Young (2004). As a first approximation of these limits, one could use $\alpha_{sup} \cong (\pi/2 - \theta)$ and $\alpha_{inf} \cong (\theta - \pi/2)$.

Using Eq. (5), the mean capillary pressure can be calculated as a function of primarily two factors: the liquid wettability (encompassing both surface tension σ and advancing contact angle θ) and geometric configuration of the porous medium (either spacing ratio ξ or solid volume fraction V_f). From this point on, we will use the phrase "capillary pressure" to designate the actual mean capillary pressure.

3.5. Boundary pressure conditions and Entrapped gas pressure

In order to integrate the governing equations of liquid impregnation from the outer surface of the permeable macro-cylinder to the center, the boundary conditions need to be specified. While the pressure outside of the macro-cylinder could be assumed known, specifying the pressure at the advancing liquid boundary is more challenging, as this depends not only on the capillary pressure at the interface, but also on the entrapped gas pressure as the liquid radially impregnates the circular domain (Fig. 4a). The actual value of liquid's pressure

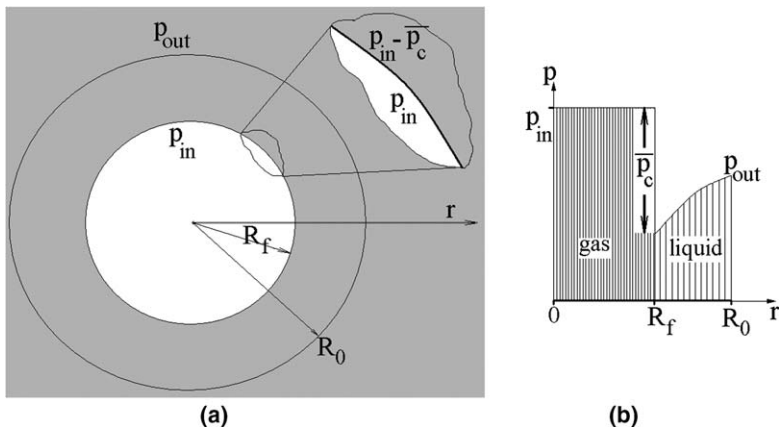

Fig. 4. (a) Pressure jump at the liquid/gas interface. The current flow front radius is R_f pressure of liquid surrounding the cylindrical porous structure is p_{out}, inside gas pressure is p_{in} and the capillary pressure is p_c. (b) Possible pressure variation for a spontaneous capillary impregnation. Flow toward the center develops as long as p_{out} is greater than the difference $(p_{in} - p_c)$ as illustrated in (b).

at the interface is equal to the difference between the gas pressure at the interface and the (mean) capillary pressure. The liquid continues to impregnate the porous medium toward the center, as long as there is a positive pressure gradient in the r-direction from the center to the outer surface. Radial liquid impregnation stops when one of the following two situations occurs: either the flow front reaches the center of the porous macro-cylinder, or the pressure outside of the porous structure ceases to offset the difference between the inner gas pressure and the capillary pressure.

The sketch in Fig. 4b exemplifies a situation where impregnation continues despite the inside gas pressure being larger than the liquid pressure outside of the macro-cylinder. It is important to underline that the comparison between the inside gas pressure and the outside liquid pressure does not bear any physical meaning and it can be misleading, since the pressure gradient is created by the difference between the pressures at the two circular liquid boundaries, $\Delta p = p_{\text{out}} - (p_{\text{in}} - \overline{p_c})$. If Δp is positive, then the pressure gradient is in the radial outward direction, which produces an inward velocity field, as described by Darcy's (1856) law:

$$u_r = -\frac{K}{\eta \cdot (1 - V_f)} \cdot \frac{dp}{dr} \tag{6}$$

where u_r is the radial liquid velocity, K is the permeability of the porous macro-cylinder in the radial direction, and η is the liquid viscosity.

The inside gas pressure can be expressed as a function of the flow front radius only, if it is assumed that the gas cannot escape or dissolve in the liquid. However, because the gas inside might dissolve in the advancing liquid, it is necessary to model the gas pressure inside to account for this possibility as expressed by the following equation:

$$\underbrace{p_{\text{in}}}_{\text{current\_gas\_pressure}} \underbrace{\cdot (\pi R_f^2 \cdot L) \cdot \underbrace{(1 - V_f)}_{\text{porosity}}}_{\substack{\text{volume\_currently} \\ \text{occupied\_by\_gas}}} = \underbrace{p_{\text{out}}|_{t=0}}_{\text{initial\_gas\_pressure}} \underbrace{\cdot (\pi R_0^2 \cdot L) \cdot \underbrace{(1 - V_f)}_{\text{porosity}}}_{\substack{\text{volume\_initially} \\ \text{occupied\_by\_gas}}} \cdot \underbrace{(1 - \lambda)}_{\substack{\text{fraction\_of} \\ \text{remaining\_gas}}} \tag{7}$$

where R_f is the flow front radius, R_0 is the radius of the porous macro-cylinder, and L is its length of the porous cylinder. Eq. (7) also includes λ, a "lumped" function, which our approach introduces to encompass the complexity of the gas displacement process. Function λ describes the fraction of gas escaped or dissolved in the liquid before the current time t, versus the total initial mass of gas trapped inside. By "correcting" the ideal gas law with function λ, seen as a "loss factor", we obtain the relationship between the pressure, p_{in} inside the porous domain and the current radial coordinate of the liquid front, R_f impregnating the cylindrical porous media:

$$p_{\text{in}} = p_{\text{out}} \cdot \left(\frac{R_0}{R_f}\right)^2 \cdot (1 - \lambda) = p_{\text{out}} \cdot \frac{(1 - \lambda)}{\varepsilon_f^2} \tag{8}$$

The new dimensionless coordinate introduced in Eq. (8) is the normalized flow front location $\varepsilon_f = R_f/R_0$, which will be the primary independent variable for the analytical integration. Our intent is not to exhaustively describe the variation of function $\lambda = \lambda(R_f, R_0, V_f, r_\mu, \eta, \sigma, \text{etc.})$ with respect to each identified factor, but rather to consider its qualitative influence on the impregnation results. The experimental extension of this paper (Part II) will attempt to quantitatively determine how the fraction of escaped gas λ varies with the material and process parameters.

General observations can be made if we explore the behavior of function λ versus the normalized flow front location, $\varepsilon_f = R_f/R_0$. The initial condition, specifying that no gas had been displaced at $t = 0$ (i.e. $\varepsilon_f = 1$) is equivalent to $\lambda(1) = 0$. Similarly, if the liquid reaches the center of the circular porous domain ($\varepsilon_f = 0$), all the gas has already dissolved or escaped out through the liquid domain which implies $\lambda(0) = 1$. From physical considerations and its definition it follows that the escaped gas fraction cannot have values outside the interval $[0; 1]$. Therefore, as ε_f decreases during the impregnation from one to zero, function $\lambda(\varepsilon_f)$ increases from zero to one.

More information can be obtained about the variation of function $\lambda(\varepsilon_f)$ only if supplementary assumptions are made. For instance, if we assume that the pressure p_{out} on the circumference of the porous macro-cylinder and the capillary pressure $\overline{p_c}$ are constant during the impregnation, then we could state the following:

- Because the infusion shrinks the gas domain, at any time during the impregnation, the gas pressure inside the porous domain (p_{in}) remains larger than the outside pressure p_{out} (also see Fig. 4a). Eq. (8) can be used to cast this property of function $\lambda(\varepsilon_f)$ into an inequality that needs to be satisfied:

$$\lambda(\varepsilon_f) \leqslant 1 - \varepsilon_f^2 \tag{9}$$

  It is implicit here that the initial pressures of the gas and in the liquid were also equal to the constant outside pressure p_{out}.
- The pressure gradient in the positive r-direction will exist only if the liquid pressure at the interface ($p_{in} - \overline{p_c}$) is lower than the outside pressure p_{out}. This is equivalent to the following inequality:

$$1 - \varepsilon_f^2 \cdot (1 + \beta) \leqslant \lambda(\varepsilon_f) \tag{10}$$

  where β is defined as the ratio between the mean capillary pressure $\overline{p_c}$ and the outside pressure p_{out}: $\beta = \overline{p_c}/p_{out}$.

The consequence of the statements above is that in the particular case of constant p_{out} and $\overline{p_c}$, the domain of possible variations of fraction of gas $\lambda(\varepsilon_f)$ that escapes or dissolves is bounded by inequalities (9) and (10). The chart in Fig. 5 displays the two limits for an arbitrary given value of β. Although the profile of curve $\lambda(\varepsilon_f)$ is not known, it has to fit in the positive region ($\lambda \geqslant 0$) delimited by curves $\lambda^{(0)}(\varepsilon_f)$ and $\lambda^{(1)}(\varepsilon_f)$. The upper limit $\lambda^{(0)}$ corresponds to the case where there are no factors inhibiting the gas escape or dissolution into the liquid, whereas the positive side of curve $\lambda^{(1)}$ describes the other limiting case: when no gas can escape or dissolve, the pressure inside continues to increase until the pressure gradient becomes null and the flow progression towards the center of the tow comes to a standstill.

3.6. Modeling dissolution or escape of entrapped gas/air

There are many ways to define the variation of an arbitrary curve $\lambda(\varepsilon_f)$, fulfilling the requirements stated above. The model we propose for the variation of escaped gas features three distinctive stages (Fig. 5), being defined by a single scalar parameter δ, which has values in the range $[0;1]$. The value of this parameter indicates two meanings. First, the parameter δ is designed as a weighing factor between the two limit curves $\lambda^{(0)}(\varepsilon_f)$ and $\lambda^{(1)}(\varepsilon_f)$, in such a way that lower values ($\delta \approx 0$) correspond to curves closer to the limit $\lambda^{(0)}(\varepsilon_f)$, whereas

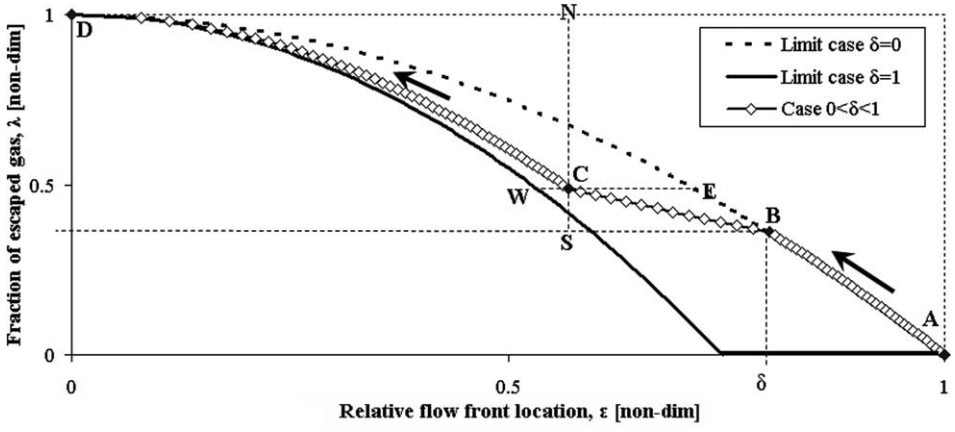

Fig. 5. The proposed variation of escaped gas $\lambda(\varepsilon_f)$ is shown for an arbitrary value of parameter δ. The curve features three stages of the gas escaping process, as proposed by the model (segments AB, BC and CD). Both axes are dimensionless.

higher values ($\delta \approx 1$) indicate approaching the limiting case $\lambda^{(1)}(\varepsilon_f)$. Secondly, the same parameter δ is the normalized radial coordinate defining the end of the first stage of the capillary impregnation (Fig. 5).

During the first stage (segment AB), the inside gas is assumed to escape at such a rate that the inside pressure p_{in} remains constant and is equal to the outside liquid pressure p_{out}. This segment overlaps with the limiting curve $\lambda^{(0)}(\varepsilon_f)$. The existence of this stage is justified by experimental investigations on capillary impregnations of porous cylindrical structures (Part II). Similar observations were made by Bernet et al. (1999), who challenges the assumption of axisymmetry during the first stage of the radial impregnation of fiber bundles in thermoplastic composites. As a consequence, the region inside the porous macro-cylinder (the fiber bundle) can be seen as a 'pore' not closed yet by the surrounding liquid during this initial stage.

During the third stage (segment CD), the flow front is assumed to advance in such a way that the fraction of escaped gas $\lambda(\varepsilon_f)$ varies as a weighed average between the two limits $\lambda^{(0)}(\varepsilon_f)$ and $\lambda^{(1)}(\varepsilon_f)$, according to the value of parameter δ.

The second stage (segment BC) is proposed as a transitional phase, ensuring continuity between the first and third segments of the curve $\lambda(\varepsilon_f)$.

As seen in Fig. 5, the resulting curve for $\lambda(\varepsilon_f)$ is the sum of three curves linking four points of coordinates $A(1;0),\ B(\delta;1-\delta^2),\ C[\delta\sqrt{\delta}\cdot(1-\delta+\delta/\sqrt{1+\beta});1-\delta^3]$ and $D(0;1)$ in Cartesian coordinates $(\varepsilon;\lambda)$.

While points A and D are easily identified as the start and end of the impregnation, respectively, additional information is needed to show how points B and C were defined. Thus, point B is defined as belonging to the limit curve $\lambda^{(0)}(\varepsilon_f)$ and being located at abscissa δ. High values of parameter δ reduce the first stage and bring point B closer to the start of the impregnation, while lower values of δ indicate that the first stage lasts longer, and B gets closer to point D on the curve $\lambda^{(0)}(\varepsilon_f)$.

After the Cartesian coordinates of point B are known, point C is further defined in the upper region between the two limit curves $\lambda^{(0)}(\varepsilon_f)$ and $\lambda^{(1)}(\varepsilon_f)$, so that its coordinates satisfy the geometric relations:

$$\frac{CN}{SN} = \frac{CE}{WE} = \delta \tag{11}$$

Lower values of parameter δ would increase the ordinate of point C, which approaches the limit curve $\lambda^{(0)}(\varepsilon_f)$. Conversely, higher values of δ move point C downward and close to the limit case $\lambda^{(1)}(\varepsilon_f)$.

The mathematical expression consistent with the above description of function $\lambda^{(\delta)}(\varepsilon_f)$ can be written as

$$\lambda = \begin{cases} 1-\varepsilon^2, & \text{if } \delta < \varepsilon \leqslant 1 \\ \lambda_{BC}(\varepsilon), & \text{if } \varepsilon_C < \varepsilon \leqslant \delta \\ 1-\delta^3\left(\dfrac{\varepsilon}{\varepsilon_C}\right)^2, & \text{if } 0 \leqslant \varepsilon \leqslant \varepsilon_C \end{cases} \tag{12}$$

where $\varepsilon_C = \delta\sqrt{\delta}\cdot(1-\delta+\delta/\sqrt{1+\beta})$ and $\lambda_{BC}(\varepsilon)$ is an intrinsic definition pertaining to the second stage of the impregnation (segment BC in Fig. 5), by means of the following equation:

$$\frac{\sqrt{1-\lambda}-\varepsilon}{\delta\sqrt{1-\lambda}\left(1-\frac{1}{\sqrt{1+\beta}}\right)} = \frac{\delta^2-(1-\lambda)}{\delta^2(1-\delta)} \tag{13}$$

An equivalent definition of function $\lambda^{(\delta)}(\varepsilon_f)$ in inverse form may be more convenient, especially for implementation in numerical codes. The following is an expression of $\varepsilon_f = f(\lambda)$:

$$\varepsilon_f = \begin{cases} \sqrt{1-\lambda}, & \text{if } 0 < \lambda \leqslant 1-\delta^2 \\ \sqrt{1-\lambda}\cdot\left[1-\delta\left(1-\dfrac{1}{\sqrt{1+\beta}}\right)^{\frac{\delta^2-1+\lambda}{\delta^2(1-\delta)}}\right], & \text{if } 1-\delta^2 < \lambda \leqslant 1-\delta^3 \\ \sqrt{1-\lambda}\cdot\left[1-\delta\left(1-\dfrac{1}{\sqrt{1+\beta}}\right)\right], & \text{if } 1-\delta^3 < \lambda \leqslant 1 \end{cases} \tag{14}$$

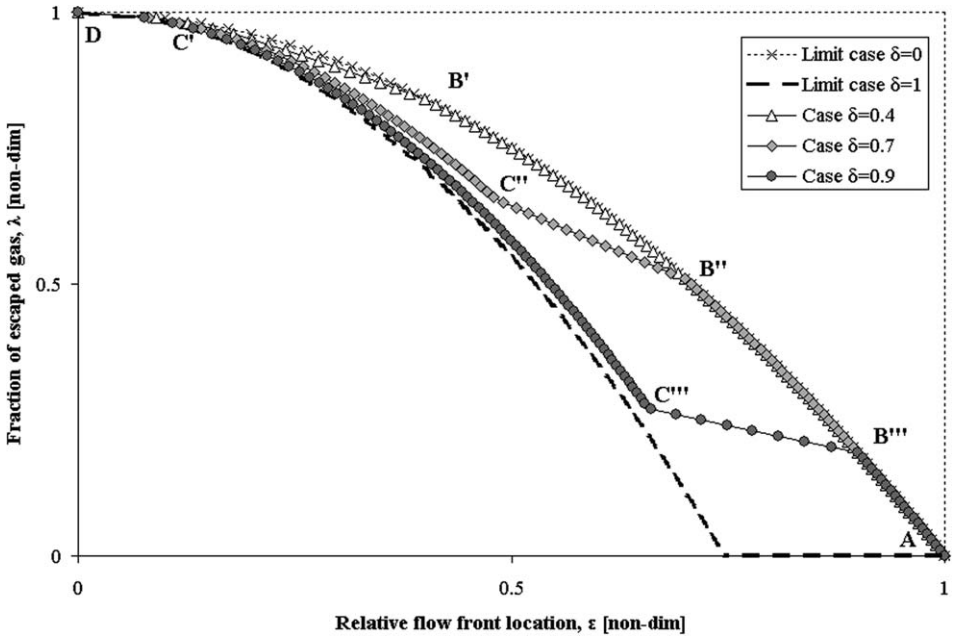

Fig. 6. Profiles of fraction of escaped and dissolved gas λ for five values of parameter δ. The lengths of the three stages of impregnation depend on the value of parameter δ and it is apparent that the limit cases do not feature all three stages. For example, if $\delta = 0$, points B, C and D coincide and only the first stage is present. Conversely, if $\delta = 1$ points B and A coincide, while point C is located on the abscissa.

Several curves $\lambda^{(\delta)}(\varepsilon_f)$ are shown in Fig. 6, for different values of parameter δ. It is interesting to observe that the definition of function $\lambda^{(\delta)}(\varepsilon_f)$ allows one to recover the two limit cases identified before, for the fraction of escaped gas. Thus, when parameter δ is zero, points B, C and D coincide and the curve $\lambda(\varepsilon_f)$ entirely overlaps with limit curve $\lambda^{(0)}(\varepsilon_f)$. On the contrary, when parameter δ is equal to unity, point B coincides with A and point C is located on the ε-axis, at the intersection of curve $\lambda^{(1)}(\varepsilon_f)$ and the abscissa.

More insight into how parameter δ affects the capillary impregnation can be gained by experimentally approaching the gas escape/dissolution phenomenon. An experimental study of how parameter δ is influenced by the geometry of the porous structure is included in Part II.

4. Results and discussion

4.1. Impregnation dynamics (relationship between flow front location and time)

Starting with the minimal set of simplifying assumptions stated in a previous section, we could write the governing equations in cylindrical coordinates, as follows:

$$\frac{\partial[r \cdot u_r(r,t)]}{\partial r} = 0 \tag{15}$$

$$u_r(r,t) = -\frac{K(r)}{\eta(t) \cdot [1 - V_f(r)]} \cdot \frac{\partial p}{\partial r} \tag{16}$$

where velocity u_r, viscosity η, solid volume fraction V_f and permeability K were allowed to vary in time or across the macro-cylinder porous domain, in both mass conservation equation [Eq. (15)] and Darcy's law [Eq. (16)].

Also, the boundary conditions assume variable pressures at $r = R_0$ and $r = R_f$:

$$\begin{aligned} p|_{R_0} &= p_{out}(t) \\ p|_{R_f} &= p_{in}(R_f) - \overline{p_c}(t, R_f) \end{aligned} \tag{17}$$

To keep a greater degree of generality, the mean capillary pressure was assumed variable due to a possible alteration of surface tension and contact angle during the impregnation, as well as due to a non-uniform distribution of the micro-cylinders within the porous macro-cylinder. Outer pressure is also allowed to vary in time. The initial pressure condition specifies that at the beginning of the impregnation, the inner gas pressure is equal to the outside liquid pressure:

$$p_{\text{in}}(R_0) = p_{\text{out}}(t=0) \tag{18}$$

The integration from the outside of the porous macro-cylinder of radius R_0 to the current flow front location R_f will lead to the following relationship between flow front radius and time:

$$[p_{\text{out}}(t) - p_{\text{in}}(R_f) + \overline{p_c}(t, R_f)]\,\mathrm{d}t + R_f \cdot \eta(t) \cdot \left[\int_{R_f}^{R_0} \frac{1 - V_f(r)}{r \cdot K(r)}\,\mathrm{d}r\right]\mathrm{d}R_f = 0 \tag{19}$$

This equation cannot be decoupled and solved analytically, unless other simplifications are made.

Numerical results can be obtained for the general case. The algorithm, starting at the outside of the macro-cylinder, $(R_f)_0 = R_0$, with imposed increments ΔR_f for the flow front radius, will allow for the iterative calculation of time increments Δt:

$$\Delta t_i^{(j)} = -\frac{\eta\left(t_i^{(j-1)}\right) \cdot \left[\int_{(R_f)_i}^{R_0} \frac{1-V_f(r)}{r \cdot K(r)}\,\mathrm{d}r\right] \cdot (R_f)_i}{p_{\text{out}}\left(t_i^{(j-1)}\right) - p_{\text{in}}((R_f)_i) + \overline{p_c}\left(t_i^{(j-1)}, (R_f)_i\right)} \cdot \Delta R_f \tag{20}$$

where at each time step (designated by subscript "i"), a series of iterations (superscript "j") is performed, to ensure convergence of the calculated time increment. The algorithm stops when the pressure difference term $\Delta P = [p_{\text{out}}(t_i) - p_{\text{in}}(R_f) + \overline{p_c}(t_i, R_f)]$ becomes zero or negative, or if $(R_f)_i$ decreases to zero (i.e. center of the porous macro-cylinder is reached). The integral in Eq. (20) can be calculated analytically, if K and V_f are constant.

A particular case of Eqs. (15)–(19) is presented by Bernet et al. (1999), who solves numerically the simplified case of uniform distribution of micro-cylinders (uniform permeability K and solid volume fraction V_f through the porous macro-cylinder). Obtaining a closed form solution is straightforward if further simplifications are made. If the liquid viscosity η and the pressure difference ΔP remain constant throughout the impregnation process, and neither solid volume fraction V_f nor permeability K vary within the porous macro-cylinder, the dynamics of the radial impregnation is given by

$$\tau = 1 - \varepsilon_f^2(1 - 2\ln\varepsilon_f) \tag{21}$$

where the non-dimensional coordinates τ and ε_f were obtained by normalizing space with respect to the macro-cylinder radius R_0 ($\varepsilon_f = R_f/R_0$) and time with respect to a characteristic time value, $t_f^{(0)}$, which is the duration of time to fully impregnate the macro-cylinder ("fill time") in this idealized case:

$$t_f^{(0)} = \frac{R_0^2 \cdot \eta \cdot (1 - V_f)}{4K \cdot \Delta P} \tag{22}$$

For comparison purposes, the dependence of space vs. time in the case of ideal impregnation is plotted in Fig. 7, along with other results (see curve $\delta = 0$). It is interesting to notice in Eq. (21), as well as in Fig. 7, that the cylindrical geometry of the medium does not allow for a simple application of the Washburn (1921) law, which states that for one-dimensional flow, there exists a linear relationship between the impregnation depth and the square root of time.

Ideal spontaneous capillary impregnation features only capillary pressure as driving factor, and therefore this is an even more restricting case, with $p_{\text{out}} = p_{\text{in}} = \text{constant}$. Relatively unrealistic, this case assumes that the inside gas does not get trapped inside and somehow manages to escape or dissolve in the impregnating liquid, at such a rate, that the inside pressure remains unchanged, and only capillarity drives the flow inward. Results similar to Eqs. (21) and (22) are obtained, with ΔP defined exclusively by the mean capillary pressure.

In this particular case, the pressure field can also be defined in normalized units, scaled with respect to the value of the outside pressure p_{out}:

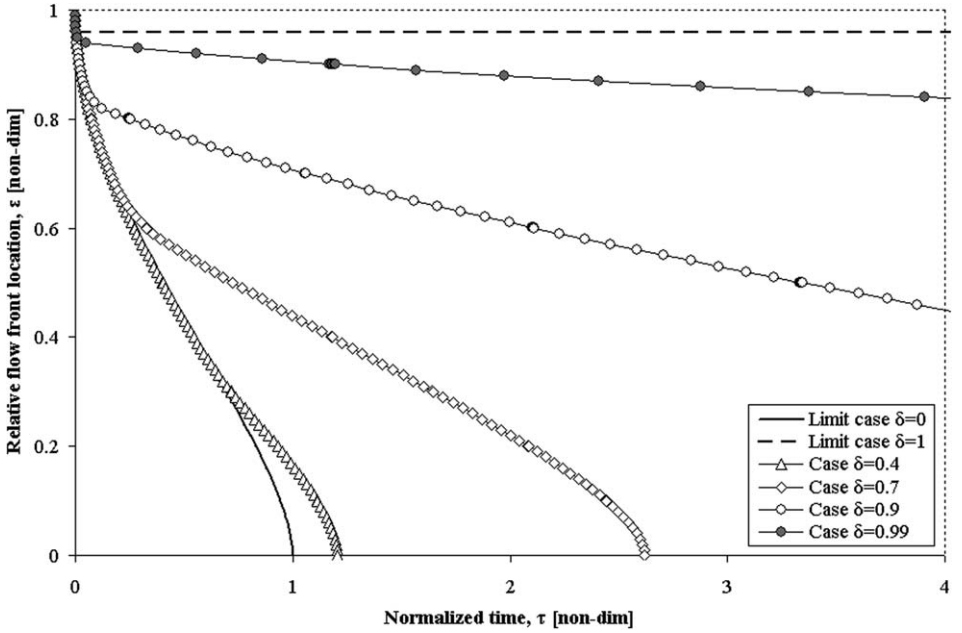

Fig. 7. Flow front advancement versus time, for several values of parameter δ. Both axes are dimensionless ($\varepsilon_f = R_f/R_0$ and $\tau = t/t_f^{(0)}$). Case $\delta = 0$ is the most favorable case for the impregnation, which takes place in the shortest time. If $\delta = 1$, the gas is compressed inside of the cylindrical porous structure during the first stage, and then impregnation stops. Any other value of δ between zero and one gives a finite impregnation time, always larger than $t_f^{(0)}$.

$$\bar{p}(\varepsilon, \varepsilon_f) = \frac{p(\varepsilon, \varepsilon_f)}{p_{out}} = 1 - \beta \cdot \frac{\ln \varepsilon}{\ln \varepsilon_f} \tag{23}$$

where factor β is the normalized capillary pressure $\beta = \bar{p}_c/p_{out}$, and $\varepsilon = r/R_0$ being a current non-dimensional radial coordinate, within the interval $[\varepsilon_f; 1]$.

Applying a similar approach, the velocity field can be written in non-dimensional form as

$$\bar{u}_r(\varepsilon, \varepsilon_f) = \frac{u_r(\varepsilon, \varepsilon_f)}{U^*} = \frac{1}{\varepsilon \cdot \ln \varepsilon_f} \tag{24}$$

where characteristic velocity U^* is defined as

$$U^* = \frac{K \cdot \overline{p_c}}{R_0 \cdot \eta \cdot (1 - V_f)} \tag{25}$$

The results expressed by Eqs. (21)–(25) were obtained for the case where gas displacement does not play any role in the impregnation process. If one takes into account this phenomenon, though, the variation of the inner gas pressure needs to be considered, by using the function of escaped/dissolved gas $\lambda(\varepsilon_f)$.

To get more insight into how the gas displacement/dissolution affect the overall capillary impregnation, a numerical computer code was written to implement the solution given by Eq. (20). Comparative plots are presented in Fig. 7 for several values of parameter δ. To facilitate comparison between different curves, all times were scaled with respect to fill time $t_f^{(0)}$, which was calculated for limit case $\delta = 0$ (no effect of gas escape/dissolution on the impregnation dynamics). In all simulations, it was assumed that the structure of the porous macro-cylinder is uniform, consequently there were no variations in the solid volume fraction V_f and permeability K of the material.

In generating the graphical results shown in Fig. 7, the rate at which the gas escapes from the center of the macro-cylinder outward is assumed to be described by Eq. (12), where an arbitrary value was attributed to the capillary pressure ratio β. It is obvious in Fig. 7 that the shortest impregnation time is achieved in the ideal case, where gas escapes easily through the liquid domain, without affecting the velocity of the flow front,

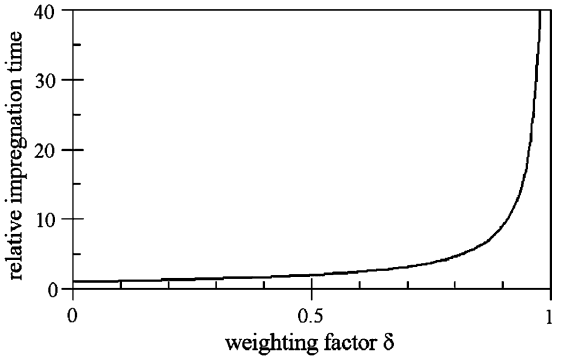

Fig. 8. Dependence of (normalized) overall impregnation time on the scalar factor δ. When δ approaches one, the case of trapped gas is recovered, whereas $\delta = 0$ corresponds to the ideal case where gas escapes/dissolves easily into the impregnating liquid, without obstructing the flow dynamics.

i.e. parameter δ is zero. At the other extreme there is the case where all gas is trapped inside with no dissolution possible (parameter δ is equal to unity). In the latter case, the flow front advances up to a certain point and stops when the pressure gradient becomes zero.

Similar conclusions could be drawn if one looks at the dependence of fill time ratio $\tau_f^{(\delta)}$ on the value of parameter δ (Fig. 8). It is apparent that higher values of the parameter δ correspond to cases where the gas displacement displays a more inhibiting effect on the impregnation process, which is consequently slowed down.

The results plotted in Figs. 7 and 8 are in non-dimensional units, independent of macro-cylinder diameter, liquid viscosity, surface tension, contact angle, solid volume fraction and permeability. However, because function $\lambda(\varepsilon_f)$ includes normalized capillary pressure ($\beta = \bar{p}_c/p_{out}$), slightly different results would be obtained for different pressure conditions. Experimental investigations on how the fraction of escaped gas λ varies in a real application are conducted and included in Part II of this paper.

4.2. Influence of local micro-cylinder distribution on the capillary impregnation

An interesting application of the numerical model described in Eqs. (15)–(20) was explored to reveal how the variation of micro-cylinder distribution within the porous macro-cylinder affects the impregnation dynamics and consequently the fill time. Spontaneous capillary impregnation within a macro-cylinder containing an average solid volume fraction (arbitrarily set at 70%), with allowance of ±10% variations of the solid volume fraction in radial direction (as shown in Fig. 9) was evaluated.

As the purpose was to study the effect of variation of solid volume fraction, no gas was considered to be entrapped within the fiber tow. The mean capillary pressure $\overline{p_c}$ and the porous medium permeability K were allowed to vary, as the solid volume fraction varied with the radial location. A numerical code was developed

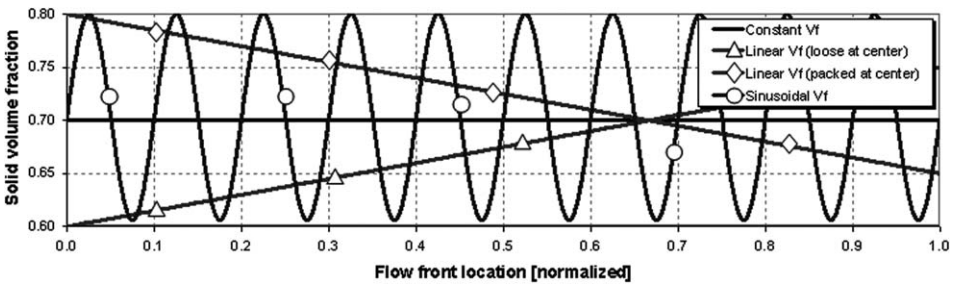

Fig. 9. The micro-cylinder distribution for the four examples included in the comparative study. All samples had the same overall solid volume fraction.

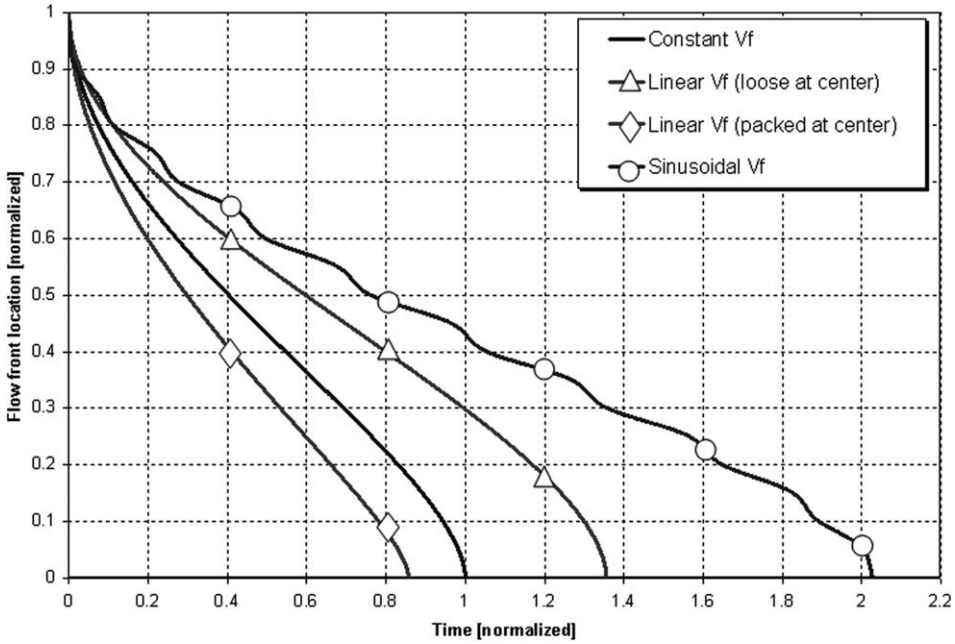

Fig. 10. Impregnation dynamics of the four porous macro-cylinders considered in the comparative study. Time is normalized with respect to the fill time obtained for uniform distribution of micro-cylinders (constant V_f).

and executed on the basis of Eq. (20) to generate the flow front radius vs. time relationship for the four similar porous samples considered, featuring equal size, equal average solid volume fraction, all impregnated by the same liquid under identical conditions.

The conclusion of this study is that even shorter fill times can be achieved, if the micro-cylinders are closer to one another at the center (higher V_f), than in the case when constant solid volume fraction is imposed. Although not included in the chart shown in Fig. 10, similar results were obtained for other types of variations of the inner micro-cylinder distribution: results for quadratic or multistep profiles for $V_f(\varepsilon_f)$ similarly indicate that denser packing at the center of the macro-cylinder leads to shorter fill times. On the contrary, if the outer region is denser than the inner region, the flow becomes slower as compared to the reference case of constant micro-cylinder distribution. Although higher local solid volume fractions V_f (i.e. lower spacing ratios ξ) yield higher capillary pressures in those regions, it seems that the effect of the much lower local permeability K prevails, therefore inducing a longer overall fill time.

A secondary conclusion that can be extended from the study is that random variations of the micro-cylinder distribution (as simulated by the sinusoidal imposed variation) increase the fill time, as compared to the fill time for a reference sample of constant solid volume fraction.

It is important to note that the direct applicability of these findings is limited, as it is still difficult to control the inner distribution of micro-cylinders in real fiber bundles, in composite or textile manufacturing. In addition to that, these conclusions were drawn for a simplified case (gas is not taken into consideration).

5. Summary and conclusions

The analytical results presented in this paper allow one to fully characterize the radial axisymmetric infusion inside a cylindrical porous domain consisting of aligned micro-cylinders. The important characteristic parameters were identified and equations were recast into non-dimensional form. To determine the rate at which the liquid impregnates the porous media created by aligned micro-cylinders, one must have the correct estimation for the porous medium permeability and be able to explicitly express the function λ describing the rate at which the gas dissolves or escapes out. It is useful to note that the results presented above can be used also for the case of a non-wetting liquid, provided that the permeation is driven by a positive applied pressure

difference. In that specific case, the equations involving contact angles and capillary pressure would need a slight revision, as some terms would become negative, capillarity playing an inhibiting role with respect to liquid motion toward the center of the porous structure.

The analytical model and its numerical extension proposed here provide a useful tool to investigate the capillary radial infusion of porous media consisting of arrays of aligned uniformly distributed micro-cylinders. The non-dimensional equations derived allow one to explore the role of gas entrapment, varying fiber volume fraction and average capillary pressure in addition to identifying characteristic values for time, pressure and velocity. The proposed technique of averaging the capillary pressure is another improvement as compared to previous analytical approaches, as it accounts for the physics of wetting at the micro-scale. Finally, the treatment of the gas displacement phenomenon requires only one parameter (δ) to be considered in order to describe the impregnation behavior of the liquid inside the circular porous domain and calculate the variations of pressure and velocity within the liquid domain.

Further experimental work, required to validate the analytical results, has been carried out by the authors and is presented in Part II.

Acknowledgments

The authors acknowledge support of their work by the AMIPC Grants N00014-02-1-0811 and N00014-03-1-0891.

References

Ahn, K.J., Seferis, J.C., Berg, J.C., 1991. Simultaneous measurements of permeability and capillary pressure of thermosetting matrices in woven fabric reinforcements. Polym. Compos. 12, 146–152.

Alazmi, B., Vafai, K., 2004. Analysis of variable porosity, thermal dispersion, and local thermal nonequilibrium on free surface flows through porous media. J. Heat Transfer 126, 389–399.

Ballata, B., Walsh, S., Advani, S.G., 1999. Measurement of the transverse permeability of fiber preforms. J. Reinforced Plast. Compos. 18, 1450–1464.

Batch, G.L., Chen, Y.-T., Macosko, C.W., 1996. Capillary impregnation of aligned fibrous beds: experiments and model. J. Reinforced Plast. Compos. 15, 1027–1051.

Bayramli, E., Powell, R.L., 1990. The normal (transverse) impregnation of liquids into axially oriented fiber bundles. J. Coll. Interf. Sci. 138, 346–353.

Bernet, N., Michaud, V., Bourban, P.-E., Månson, J.-A.E., 1999. An impregnation model for the consolidation of thermoplastic composites made from commingled yarns. J. Compos. Mater. 33, 751–772.

Binetruy, C., Hilaire, B., Pabiot, J., 1997. The interactions between flows occurring inside and outside fabric tows during RTM. Compos. Sci. Technol. 57, 587–596.

Bruschke, M.V., Advani, S.G., 1993. Flow of generalized newtonian fluids across a periodic array of cylinders. J. Rheol. 37, 479–498.

Calado, V.M.A., Advani, S.G., 1996. Effective permeability of multi-layer preforms in resin transfer molding. Compos. Sci. Technol. 56, 519–531.

Chwastiak, S., 1971. A wicking method for measuring wetting properties of carbon yarns. J. Coll. Interf. Sci. 42, 298–309.

Darcy, H., 1856. Les Fontaines publiques de la ville de Dijon. Delmont, Paris.

Dimitrovova, Z., Advani, S.G., 2002. Analysis and characterization of relative permeability and capillary pressure for free surface flow of a viscous fluid across an array of aligned cylindrical fibers. J. Coll. Interf. Sci. 245, 325–337.

Foley, M.E., 2003. The microflow behavior and interphase characterization of fiber reinforced polymer composites. Ph.D. Newark, University of Delaware.

Foley, M.E., Gillespie, J.W., 2005. Modeling the effect of fiber diameter and fiber bundle count on tow impregnation during liquid molding processes. J. Compos. Mater. 39, 1045–1065.

Gebart, B.R., 1992. Permeability of unidirectional reinforcements for RTM. J. Compos. Mater. 26, 1100–1133.

Gokce, A., Hsiao, K.T., Advani, S.G., 2002. Branch and bound search to optimize injection gate locations in liquid composite molding processes. Composites Part A: Appl. Sci. Manufact. 33, 1263–1272.

Greenberg, M.D., 1998. Advanced Engineering Mathematics. Prentice-Hall, Upper Saddle River, NJ.

Kaviany, M., 1995. Principles of Heat Transfer in Porous Media. Springer-Verlag, New York.

Lawrence, J.M., 2002. An approach to couple mold design and on-line control to manufacture complex composite parts by resin transfer molding. Composites: Part A 33, 981–990.

Liu, B., Bickerton, S., Advani, S.G., 1996. Modelling and simulation of resin transfer moulding (RTM) – gate control venting and dry spot prediction. Composites Part A: Appl. Sci. Manufact. 27, 135–141.

Lucas, R., 1918. Veber das Zeitgesetz des kapillaren aufstiegs von flussigkeiten. Kolloid Zeit. 23, 15–22.

Nedanov, P.B., Advani, S.G., 2002. A method to determine 3D permeability of fibrous reinforcements. J. Compos. Mater. 36, 241–254.

Papathanasiou, T.D., 2001. Flow across structured fiber bundles: a dimensionless correlation. Int. J. Multiphase Flow 27, 1451–1461.
Parnas, S. et al., 1994. The interaction between micro- and macro-scopic flow in RTM preforms. Compos. Struct. 27, 93–107.
Parnas, R.S., Howard, J.G., Luce, T.L., Advani, S.G., 1995. Permeability characterization. Part 1. A proposed standard reference fabric for permeability. Polym. Compos. 16, 429–445.
Pillai, K.M., Advani, S.G., 1995. Numerical and analytical study to estimate the effect of two length scales upon the permeability of a fibrous porous medium. Trans. Porous Media 21, 1–17.
Potter, K., 1997. Resin Transfer Moulding. Chapman & Hall, London.
Ranganathan, S., Phelan, F.R., Advani, S.G., 1996. A generalized model for the transverse fluid permeability in unidirectional fibrous media. Polym. Compos. 17, 222–230.
Sadiq, T.A.K., Advani, S.G., Parnas, R.S., 1995. Experimental investigation of transverse flow through aligned cylinders. Int. J. Multiphase Flow 21, 755–774.
Simacek, P., Advani, S.G., 1996. Permeability model for a woven fabric. Polym. Compos. 17, 887–899.
Simacek, P., Advani, S.G., 2003. A numerical model to predict fiber tow saturation during liquid composite molding. Compos. Sci. Technol. 63, 1725–1736.
Srinivasan, V., Vafai, K., 1994. Analysis of linear encroachment in two-immiscible fluid systems in a porous medium. ASME J. Fluids Eng. 116, 135–139.
Washburn, E.W., 1921. The dynamics of capillary flow. Phys. Rev. 17, 273–283.
Young, W.-B., 2004. Capillary impregnation into cylinder banks. J. Coll. Interf. Sci. 273, 576–580.